Chinese Chemical Letters 33 (2022) 358–361

Contents lists available at ScienceDirect

Chinese Chemical Letters

journal homepage: www.elsevier.com/locate/cclet

Mechanism of water oxidation catalyzed by vitamin B_{12}: Redox non-innocent nature of corrin ligand and crucial role of phosphate

Ying-Ying Li, Rong-Zhen Liao*

Key Laboratory of Material Chemistry for Energy Conversion and Storage, Ministry of Education, Hubei Key Laboratory of Bioinorganic Chemistry and Materia Medica, Hubei Key Laboratory of Materials Chemistry and Service Failure, School of Chemistry and Chemical Engineering, Huazhong University of Science and Technology, Wuhan 430074, China

ARTICLE INFO

Article history:
Received 6 April 2021
Revised 30 May 2021
Accepted 9 June 2021
Available online 16 June 2021

Keywords:
Water oxidation
DFT calculations
Mechanism
Vitamin B_{12}
Cobalt

ABSTRACT

Vitamin B_{12} (macrocyclic cobalamin) has been recently reported to be capable of electrochemically catalyzing water oxidation in a neutral phosphate buffer solution. In this work, density functional calculations were employed to elucidate the water oxidation mechanism catalyzed by vitamin B_{12}. The calculations showed that the catalytic cycle starts from the $L^{\bullet}$-Co^{II}-OH_2 complex **1**. A proton-coupled electron transfer process then leads to the formation of a $L^{\bullet}$-Co^{III}-OH complex **2**, followed by another proton-coupled electron transfer event to afford a corrin ligand radical cation intermediate **3** ($L^{\bullet}$-Co^{III}-$O^{\bullet}$). The redox non-innocent nature of the corrin ligand plays an essential role in the oxidation process. **3** is capable of triggering the O-O bond formation *via* a water nucleophilic attack mechanism, in which a hydrophosphate dianion functions as a base to accept a proton from the water nucleophile. A dioxygen molecule is released after the oxidation of the Co^{III}-OOH intermediate. The rate-determining step was calculated to be the O-O bond formation with a total barrier of 16.5 kcal/mol. While the use of water molecules as the proton acceptor was found to be less feasible for the O-O bond formation, with a barrier of 31.2 kcal/mol, further highlighting the crucial of phosphate in water oxidation.

Nowadays, the energy crisis is one of the urgent issues faced by us. Sunlight-driven water splitting in artificial photosystem provides a promising strategy for sustainable and clean hydrogen fuel production [1–5]. Water oxidation is a half and crucial step in water splitting, consisting of releasing four protons and four electrons and dissociating the molecular dioxygen. During the last few decades, extraordinary efforts have been devoted to this challenging reaction [6–12]. Ru-based water oxidation catalysts (WOCs) are most studied among homogeneous water oxidation communities [13–25]. However, considering the cost, low toxicity and availability, first-row transition metal-based complexes are believed to be better candidates for WOCs. Even though significant progress has been made in this field [24–32], the ultimate goal of application in artificial photosystem still needs more efficient, stable and robust WOCs. To achieve this goal, a thorough mechanistic understanding by combing experiments and computation is essential. Quantum chemical calculations are playing more and more critical roles in this area [33–35].

The commercially available vitamin B_{12} has been reported to be an environmentally friendly catalyst for chemical reactions, such as dehalogenation, CO_2 electrochemical reduction, hydrogenation of double bonds [36–39]. Because of the nontoxic and rich redox chemical property, vitamin B_{12} has attracted more and more attention in the catalytic community. Recently, Verpoort and coworkers reported that vitamin B_{12} could function as a homogeneous WOC electrochemically in pH 7.0 phosphate buffer (NaPi) solution with an overpotential of 0.58 V [40]. UV-vis, ESI-MS and FTIR experiments suggested that the catalyst remains its molecular structure up to 11 h [40]. The onset potential was observed at 1.2 V *vs.* Ag/AgCl, together with a more significant current density of water oxidation at around 1.5 V *vs*. Ag/AgCl. The linear relationship between the catalytic current and the catalyst concentration was also established, indicating a unimolecular mechanism. Furthermore, the increase of the concentration of NaPi leads to the linear growth of the current density in the working conditions, which suggested that phosphate ions may play an essential role in water oxidation [40].

In the present work, DFT calculations were used to investigate the mechanism of water oxidation catalyzed by vitamin B_{12} and address the role of phosphate ion in this chemical process. The

* Corresponding author.
E-mail address: rongzhen@hust.edu.cn (R.-Z. Liao).

https://doi.org/10.1016/j.cclet.2021.06.028
1001-8417/

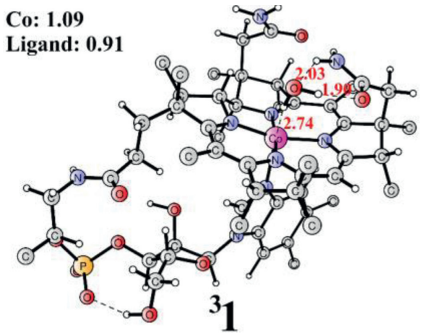

Fig. 1. Optimized structures of **1**. Distances are shown in Å in red. Mulliken spin densities on selected atoms are shown in black. The multiplicity is shown in superscript. Hydrogen atoms of methyl are not shown for clarity.

methods used here are to a large extent similar to those in our previous water oxidation studies [33,41,42], and the details are shown in Supporting information. To construct the whole energy diagram, a reference potential of 1.72 V *vs*. SHE (corresponding to 1.5 V *vs*. Ag/AgCl) was used.

We first investigated the penta-coordinated complex **1** (Co^{III}-OH_2, Fig. 1). The corrin ring has four nitrogen atoms coordinating with the cobalt center in the equatorial positions. An imidazole nitrogen atom is interacting with the metal center in the axial direction. The axial water molecule does not coordinate with the metal, instead interacts with the complex *via* two hydrogen bonds with the amide group of the ligand (Fig. 1). These two hydrogen bond distances are 2.03 and 1.90 Å, respectively. **1** prefers to be a triplet, while the singlet lies at +5.5 kcal/mol relative to the triplet. As shown in Fig. 1 and Fig. S2 (Supporting information), the spin density in **1** is partially delocalized on the ligand (total spin density of 0.91). Even though the formal oxidation state of the metal is Co^{III}, the electronic structure of **1** ($L^{\bullet}$-Co^{II}) would be better described as a low-spin Co^{II} center ($S_{Co} = 1/2$) interacting with a corrin ligand radical cation ($S_L = 1/2$). The coordination of water to cobalt to form a hexa-coordinated complex **1'** (Fig. S3 in Supporting information) is 3.6 kcal/mol higher in energy.

The oxidation of **1** to form **2** (formally Co^{IV}-OH, Fig. S4 in Supporting information) is coupled with the release of one proton from the water ligand, since the pK_a of $\mathbf{2_{pt}}$ (the protonated form of **2**, Fig. S2) was calculated to be -5.9. **2** is a doublet with the quartet state lying at +16.3 kcal/mol. The redox potential was calculated to be 0.99 V. Taking 1.72 V as a reference, this step is exergonic by 16.8 kcal/mol (Fig. 2). The spin delocalization on the ligand (spin density of 1.25) in **2** indicates that its electronic structure ($L^{\bullet}$-Co^{III}-OH) can be described as a low-spin Co^{III} ($S_{Co} = 0$) with a ligand radical cation ($S_L = 1/2$) (Fig. S2). The Co-O1 bond is 1.88 Å in **2**.

Next, a proton-coupled electron transfer (PCET) process of **2** leads to the generation of **3** (formally Co^{V}=O, Fig. S3) with a redox potential of 1.69 V. The calculated value is fully consistent with the experimental observation of 1.72 V [40]. The pK_a of $\mathbf{3_{pt}}$ (the protonated form of **3**) was calculated to be 1.8 (Fig. S2, $\mathbf{3_{pt}}$). The Mulliken spin population analysis (1.0 on the corrin and 1.0 on O1) suggested that the electronic structure of **3** ($L^{\bullet}$-Co^{III}-$O^{\bullet}$) can be interpreted as a low-spin Co^{III} ($S_{Co} = 0$) interacting with an oxyl radical ($S_O = 1/2$) as well as a ligand radical ($S_L = 1/2$) ferromagnetically, which is reminiscent of previously reported, cobalt hangmancorroles WOC [43,44]. **3** is a triplet, while the broken-symmetry singlet is slightly higher in energy, locating at +0.8 kcal/mol above. The Co-O1 distance in **3** is 1.81 Å which is somewhat shorter than that in **2**.

The formally Co^{V}=O species has been widely proposed to trigger the O-O bond formation for cobalt-based WOCs [34,44–47]. Here, two possible mechanistic scenarios for the O-O bond formation were explored. First, a water molecule performs the nucleophilic attack on the oxyl moiety of **3** to form the O-O bond, during which one proton is transferred from the attacking water molecule to phosphate ion, either HPO_4^{2-} or $H_2PO_4^-$ in working conditions (vide infra). The use of phosphate as a base has been suggested by the experiment and other metal-based water oxidation processes [34,46–50]. Second, water molecules in the aqueous solution could also function as a proton acceptor.

The transition state (**TS1**) for the water nucleophilic attack (WNA) pathway with the HPO_4^{2-} behaving as a proton acceptor is shown in Fig. 2. **TS1** prefers to be a broken-symmetry singlet, and a spin crossing from the triplet to the broken-symmetry singlet is required to prompt the O-O bond formation. In **TS1**, the atomic spin density on the oxyl radical is 0.49α, while the ligand has the opposite spin density of 0.53β, which provides the most efficient electronic state for the O-O bond formation. (Fig. 2) During the O-O bond formation, the attacking water molecule provides a pair of electrons to form the O-O bond [33,51]. The α-electron from the nucleophilic water molecule transfers to the ligand, while the proton is transferred to the phosphate. This can be considered an uncommon PCET process in which proton and electron are delivered to different acceptors. The β-electron left could easily combine with the oxyl radial to afford the O-O bond, which is similar to our previous work on the iron WOC [41]. **TS1** was confirmed to have only one imaginary frequency of 1237.2 i cm^{-1}, which corresponds to the O-O bond formation and proton transfer from water to phosphate. At **TS1**, the nascent O1-O2 bond distance is 1.96 Å. **TS1** has a barrier of +16.5 kcal/mol above the **3**. The triplet state lies at +9.5 kcal/mol relative to the broken-symmetry singlet. Downhill from **TS1**, the singlet intermediate **Int1** with a hydroperoxide coordinated to Co^{III} (Fig. S4) is generated. In **Int1**, the O1-O2 bond length is 1.45 Å, and the Co-O1 distance increases from 1.81 Å in **3** to 1.83 Å in **Int1**. **Int1** lies at +4.6 kcal/mol relative to **3**. When $H_2PO_4^-$ was used as the proton acceptor, the barrier was calculated to be 17.9 kcal/mol (**TS1'**, Fig. 2), which is 1.4 kcal/mol higher than the HPO_4^{2-} assisted pathway. The NBO calculations were carried out for the transition states, and the NBO charge for HPO_4^{2-} moiety in **TS1** is −1.75, while in **TS1'** the charge is calculated to be −0.84 for $H_2PO_4^-$ moiety (Table S2 in Supporting information). This explains the favorability for the former pathway for WNA. In **TS1'**, the O1-O2 distance is 0.03 Å shorter than that in **TS1**. In the working condition (pH 7.0, 0.1 mol/L NaPi), the concertation of $H_2PO_4^-$ and HPO_4^{2-} are 0.062 mol/L and 0.038 mol/L, respectively. In any case, the HPO_4^{2-} assisted pathway is preferred.

Alternatively, the transition state (**TS1"**) with water molecules featuring as the proton acceptor is shown in Fig. 2. In this configuration, three more water molecules were added to solvate the generated hydronium explicitly [41,52,53]. **TS1"** was confirmed as a real transition state with only one imaginary frequency of 610.7 i cm^{-1}. **TS1"** prefers to be a broken-symmetry singlet, in which the oxyl radical and the corrin ligand have opposite spin populations (0.44 on the oxyl, while -0.44 on the ligand). The crucial O1-O2 distance is 1.89 Å at **TS1"**. The Co- O1 length increases to 1.86 Å from 1.81 Å in **3**. The O2-H1 and O4-H1 distances are 1.02 Å and 1.58 Å, respectively. The barrier for this pathway was calculated to be 31.2 kcal/mol, which is much higher than the phosphate pathway (Fig. 2). The triplet **TS1"** was calculated to be 8.5 kcal/mol higher than the broken singlet. This WNA process also generated the hydro-peroxide intermediate **Int1**, which joins the previous pathway.

From **Int1**, a PECT process leads to the formation of **Int2** (Fig. S6 in Supporting information) with a redox potential of only 0.13 V. This demonstrated that this oxidation process is quite facile, with an exergonicity of 36.7 kcal/mol (Fig. 2). **Int2** is a quartet state, while the doublet state is 3.0 kcal/mol higher. In **Int2**, the triplet dioxygen is already generated since the spin densities on O1 and

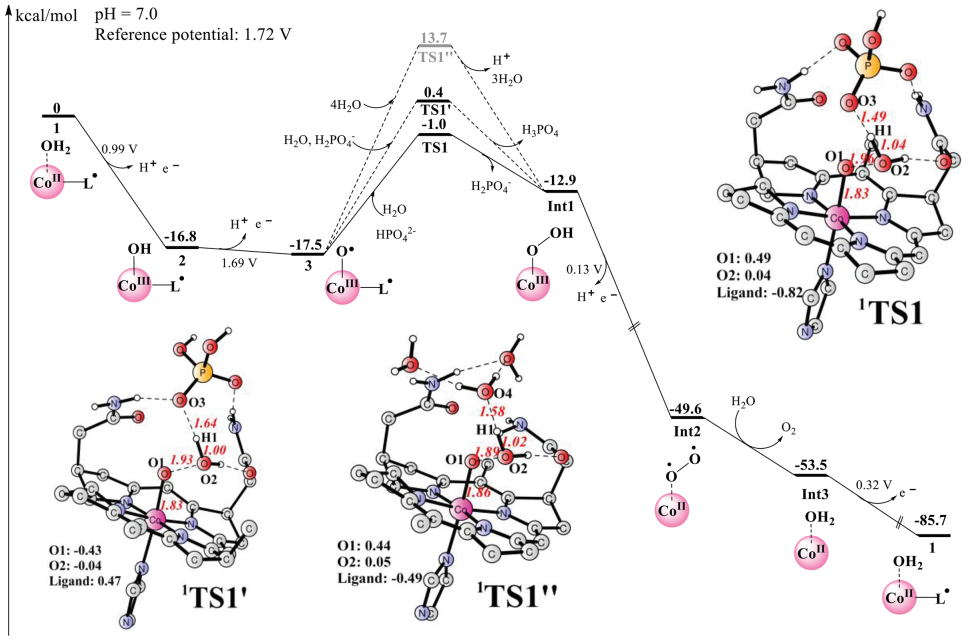

Fig. 2. Gibbs energy profile for water oxidation at the B3LYP-D3 level. Optimized **TS1** (top right), **TS1'** and **TS1"** (bottom left) in broken singlet are also shown. The imaginary frequencies of **TS1, TS1'** and **TS1"** were 1237.2 *i* cm^{-1}, 1164.0 *i* cm^{-1} and 610.7 *i* cm^{-1}, respectively. Some of the unimportant atoms are not shown for clarity. Distances are shown in Å in red. Mulliken spin densities on selected atoms are shown in black.

O2 are 0.95 and 0.99, respectively. Meanwhile, the O_2 dissociates from the cobalt center with the calculated Co-O1 distance of 3.26 Å. Furthermore, during the oxidation process, one electron is transferred from the hydro-peroxide moiety to the Co center with the formation of a low spin Co^{II}, whose spin density is 0.99 (Fig. S4). The release of O_2 from **Int2** is followed by the binding of a water molecule to form the doublet intermediate **Int3** (Fig. S4), with the quartet 12.1 kcal/mol higher in energy. This ligand exchange process is exergonic by 4.0 kcal/mol (Fig. 2). Finally, the last one-electron oxidation process from **Int3** regenerates **1**, with a calculated redox potential of 0.32 V. It should be mentioned that the ligand is involved in this oxidation process, as the spin is partially delocalized on the ligand in **1** ($L^{\bullet}$-Co^{II}).

From Fig. 2, it can be seen that the O-O bond formation is the rate-determining step with a calculated total barrier of 16.5 kcal/mol at the B3LYP-D3 level. It should be mentioned that the use of different applied potentials may change the total barrier. When using a reference potential lower than 1.69 V (oxidation potential of **2** to **3**), the total barrier will increase somewhat as the formation of **3** becomes endergonic. For example, when a reference potential of 1.4 V was used to set up the energy diagram, the total barrier increases to 23.2 kcal/mol (Table S1 in Supporting information). If the reference potential is higher than 1.69 V, the total barrier does not change as the formation of **3** is exergonic. **3** is the resting state for the O-O bond formation and its electronic structure is $L^{\bullet}$-Co^{III}-$O^{\bullet}$. Therefore, the catalytic activity of water oxidation is assisted by the redox non-innocent corrin ligand, which avoids the access of the high-valent metal center. The use of non-innocent ligands has been disclosed in other metal-based WOCs, a beneficial strategy in the catalytic water oxidation process [11,41,48,54]. Furthermore, single-point calculations were performed using the MN15 and MN15L functionals [55,56]. The calculated redox potentials and total barriers are summarized in Table 1. For the first oxidation process, the MN15 gives a relatively higher redox potential value than B3LYP-D3 and MN15L. Importantly, all functionals give similar results for the O-O bond formation. When HPO_4^{2-} was used to accept the proton, the barrier is 14.7 kcal/mol lower than water receiving the proton at the B3LYP-D3 level. The barrier differences at the MN15 and MN15L levels are 16.9 kcal/mol and 18.9 kcal/mol, respectively. This demonstrated that HPO_4^{2-} is a better base for the O-O bond formation in the water oxidation process.

Table 1
Comparison of redox potentials and total barriers at different levels.[a]

Functionals	Co^{III}/Co^{IV}	Co^{IV}/Co^{V}	WNA[b]	WNA[c]
B3LYP-D3	0.99	1.69	16.5	31.2
MN15	1.52	1.63	22.7	39.6
MN15L	0.86	1.45	20.1	39.0

[a] Redox potentials are given in V, and energies are given in kcal/mol.
[b] WNA mechanism with phosphate ion working as the proton acceptor.
[c] WNA mechanism with water working as the proton acceptor.

To conclude, we provide insights into the mechanism of water oxidation catalyzed by commercially available cobalamin (vitamin B_{12}) through density functional calculations. The suggested catalytic cycle is summarized in Scheme 1, and the corresponding energy diagram is shown in Fig. 2. The starting point of the catalytic cycle is the formal Co^{III}-OH_2 complex **1**. Two sequential PCET processes result in the formation of a formal Co^{V}=O intermediate **3**, which can be described as $L^{\bullet}$-Co^{III}-$O^{\bullet}$. The redox non-innocent character of the corrin ligand in the water oxidation was illuminated. **3** initiates the O-O bond formation *via* WNA with the production of a hydro-peroxide intermediate. Importantly, HPO_4^{2-} in the phosphate buffer was suggested to be the proton acceptor during the O-O bond formation. This step was suggested to be rate-determining with a total barrier of 16.5 kcal/mol. The alternative pathway with water accepting the proton during the O-O bond formation was calculated to be kinetically unfavorable since the barrier is 14.7 kcal/mol higher. The triplet dioxygen molecule dissociated from the cobalt center spontaneously after one PCET process from the Co^{III} hydro-peroxide intermediate. Finally, the second water molecule enters after the release of O_2, followed by another one-electron oxidation process to regenerate **1**.

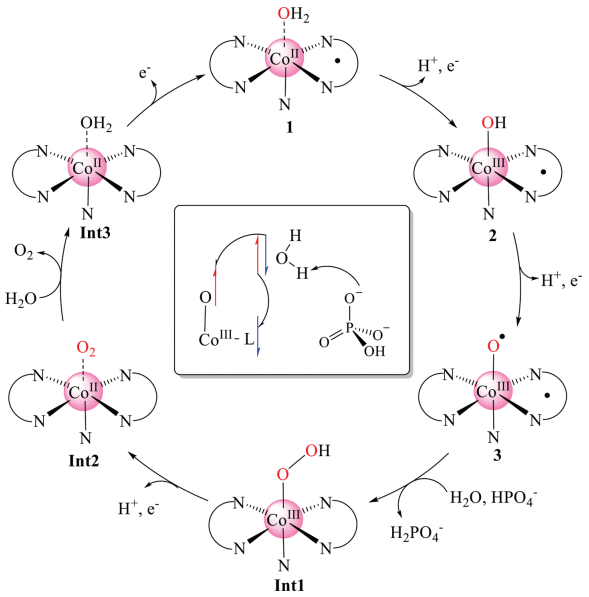

Scheme 1. Suggested water oxidation mechanism. Inset: The electron flow during the O-O bond formation is described.

Declaration of competing interest

All authors declare that no conflict of interest exists.

Acknowledgments

This work was supported by the National Natural Science Foundation of China (No. 21873031) and the National Key R&D Program of China (No. 2018YFA0903500).

Supplementary materials

Supplementary material associated with this article can be found, in the online version, at doi:10.1016/j.cclet.2021.06.028.

References

[1] B. Zhang, L. Sun, Chem. Soc. Rev. 48 (2019) 2216–2264.
[2] N. Wang, H. Zheng, W. Zhang, R. Cao, Chin. J. Catal. 39 (2018) 228–244.
[3] M.D. Karkas, B. Akermark, Dalton Trans. 45 (2016) 14421–14461.
[4] M.D. Karkas, O. Verho, E.V. Johnston, B. Akermark, Chem. Rev. 114 (2014) 11863–12001.
[5] Y. Yang, Y. Tang, H. Jiang, et al., Chin. Chem. Lett. 30 (2019) 2089–2109.
[6] Q. Han, Y. Ding, Dalton Trans. 47 (2018) 8180–8188.
[7] P. Garrido-Barros, C. Gimbert-Surinach, R. Matheu, X. Sala, A. Llobet, Chem. Soc. Rev. 46 (2017) 6088–6098.
[8] J.D. Blakemore, R.H. Crabtree, G.W. Brudvig, Chem. Rev. 115 (2015) 12974–13005.
[9] B.M. Hunter, H.B. Gray, A.M. Muller, Chem. Rev. 116 (2016) 14120–14136.
[10] H. Wang, S. Zhu, J. Deng, et al., Chin. Chem. Lett. 32 (2021) 291–298.
[11] G. Wang, Z. Li, W. Wu, et al., Phys. Chem. Chem. Phys. 22 (2020) 24446–24454.
[12] G. Wang, Y. Zhi, L. Xia, et al., Phys. Status Solidi A 217 (2020) 1900859.
[13] N. Vereshchuk, R. Matheu, J. Benet-Buchholz, et al., J. Am. Chem. Soc. 142 (2020) 5068–5077.
[14] S. Zhan, J.A. De Gracia Trivino, M.S.G. Ahlquist, J. Am. Chem. Soc. 141 (2019) 10247–10252.
[15] Q. Daniel, L. Duan, B.J.J. Timmer, et al., ACS Catal. 8 (2018) 4375–4382.
[16] R. Matheu, M.Z. Ertem, J. Benet-Buchholz, et al., J. Am. Chem. Soc. 137 (2015) 10786–10795.
[17] S. Neudeck, S. Maji, I. Lopez, et al., J. Am. Chem. Soc. 136 (2014) 24–27.
[18] L. Duan, F. Bozoglian, S. Mandal, et al., Nat. Chem. 4 (2012) 418–423.
[19] D.J. Wasylenko, C. Ganesamoorthy, M.A. Henderson, et al., J. Am. Chem. Soc. 132 (2010) 16094–16106.
[20] S.W. Kohl, L. Weiner, L. Schwartsburd, et al., Science 324 (2009) 74-44.
[21] L. Duan, A. Fischer, Y. Xu, L. Sun, J. Am. Chem. Soc. 131 (2009) 10397–10399.
[22] J.J. Concepcion, J.W. Jurss, J.L. Templeton, T.J. Meyer, J. Am. Chem. Soc. 130 (2008) 16462–16463.
[23] R. Zong, R.P. Thummel, J. Am. Chem. Soc. 127 (2005) 12802–12803.
[24] C. Sens, I. Romero, M. Rodriguez, et al., J. Am. Chem. Soc. 126 (2004) 7798–7899.
[25] J.A. Gilbert, D.S. Eggleston, W.R. Murphy, et al., J. Am. Chem. Soc. 107 (1985) 3684-3670.
[26] Y. Li, R. Yao, Y. Chen, et al., Catalysts 10 (2020) 1–20.
[27] G. Maayan, N. Gluz, G. Christou, Nat. Catal. 1 (2018) 48–54.
[28] M. Okamura, M. Kondo, R. Kuga, et al., Nature 530 (2016) 465–468.
[29] P. Garrido-Barros, D. Moonshiram, M. Gil-Sepulcre, et al., J. Am. Chem. Soc. 142 (2020) 17434–17446.
[30] H.Y. Du, S.C. Chen, X.J. Su, L. Jiao, M.T. Zhang, J. Am. Chem. Soc. 140 (2018) 1557–1565.
[31] H. Lee, X. Wu, L. Sun, ChemSusChem 13 (2020) 3277–3282.
[32] L. Wang, L. Duan, R.B. Ambre, et al., J. Catal. 335 (2016) 72–78.
[33] R.Z. Liao, P.E.M. Siegbahn, ChemSusChem 10 (2017) 4236–4263.
[34] M. Schilling, S. Luber, Front. Chem. 6 (2018) 1–21.
[35] A.V. Marenich, J. Ho, M.L. Coote, C.J. Cramer, D.G. Truhlar, Phys. Chem. Chem. Phys. 16 (2014) 15068–15106.
[36] M. Giedyk, K. Goliszewska, D. Gryko, Chem. Soc. Rev. 44 (2015) 3391–3404.
[37] K.L. Brown, Chem. Rev. 105 (2005) 2075–2149.
[38] R. Banerjee, S.W. Ragsdale, Annu. Rev. Biochem. 72 (2003) 209–247.
[39] J. Chen, C. Karin, V.K. Priyank, et al., ACS Appl. Mater. Interfaces 12 (2020) 41288–41293.
[40] H.M. Shahadat, H.A. Younus, N. Ahmad, et al., Chem. Commun. 56 (2020) 1968–1971.
[41] Y.Y. Li, L.P. Tong, R.Z. Liao, Inorg. Chem. 57 (2018) 4590–4601.
[42] R.Z. Liao, S. Masaoka, P.E.M. Siegbahn, ACS Catal. 8 (2018) 11671–11678.
[43] D.K. Dogutan, J.R. McGuire, D.G. Nocera, J. Am. Chem. Soc. 133 (2011) 9178–9180.
[44] M.Z. Ertem, C.J. Cramer, Dalton Trans. 41 (2012) 12213–12219.
[45] A. Fernando, C.M. Aikens, J. Phys. Chem. C 119 (2015) 11072–11085.
[46] W. Lai, R. Cao, G. Dong, et al., J. Phys. Chem. Lett. 3 (2012) 2315–2319.
[47] H. Lei, A. Han, F. Li, et al., Phys. Chem. Chem. Phys. 16 (2014) 1883–1893.
[48] J. Shi, Y.H. Guo, F. Xie, Q.F. Chen, M.T. Zhang, Angew. Chem. Int. Ed. 59 (2020) 4000–4008.
[49] M.K. Coggins, M.T. Zhang, Z. Chen, N. Song, T.J. Meyer, Angew. Chem. Int. Ed. 53 (2014) 12226–12230.
[50] H. Pan, L. Duan, R.Z. Liao, ChemCatChem 12 (2019) 219–226.
[51] D.W. Shaffer, Y. Xie, J.J. Concepcion, Chem. Soc. Rev. 46 (2017) 6170–6193.
[52] R.Z. Liao, X.C. Li, P.E.M. Siegbahn, Eur. J. Inorg. Chem. 4 (2014) 728–741.
[53] M.Z. Ertem, L. Gagliardi, C.J. Cramer, Chem. Sci. 3 (2012) 1293-129.
[54] T. Wada, K. Tsuge, K. Tanaka, Inorg. Chem. 40 (2001) 329–337.
[55] H.S. Yu, X. He, D.G. Truhlar, J. Chem. Theory Comput. 12 (2016) 1280–1293.
[56] H.S. Yu, X. He, S.L. Li, D.G. Truhlar, Chem. Sci. 7 (2016) 5032–5051.